JOURNAL OF MATERIALS SCIENCE 31 (1996) 4679–4687

The shrinkage compensation of unsaturated polyester resins – polyvinyl acetate blends polymerization proceeds through fractal morphologies: characterization and simulation

M. RUFFIER, G. MERLE*, J. P. PASCAULT
Laboratoire des Matériaux Macromoléculaires, Bât. 403, URA CNRS n° 507, INSA de Lyon, 69621 Villeurbanne Cedex, France

H. BOULEÇANE, N. VINCENT
Modélisation des Systèmes et Reconnaissance des Formes (LISPI), Bât 403, INSA de Lyon, 69621 Villeurbanne Cedex, France

Blends of unsaturated polyester, styrene and polyvinyl acetate are hot cured either between glass plates or under pressure in a molding simulator. The morphologies of the products are observed using microscopy and show their usual aspects. They are characterized according to fractal concepts by image processing; the influence of mixture composition, pressure and temperature is investigated. Based on the hypothesis that phase separation governs the shrinkage compensation, a computer simulation of the fissuration phenomenon is performed using the diffusion limited agregation (DLA) model. This fractal model gives realistic results, and is used to show the effect of network parameters on the fissures fractal dimensions.

1. Introduction

The blend of unsaturated polyester (UP) prepolymer and styrene (S) is the most widely used resin for SMC (sheet molding compound) and BMC (bulk molding compound) applications. It has been known for twenty years that the addition of a thermoplastic in polyester based systems reduces most of the molding problems such as poor surface appearance, inability to mold to close tolerances and warpage of molded parts. The cause of these problems has been partially attributed to the high polymerization shrinkage during cure [1]. The mechanisms by which the thermoplastics polyvinylacetate (PVAc), polymethylmethacrylate (PMMA) and polystyrene (PS), compensate for the shrinkage are not yet well understood. Since 1975, many researchers have tried to extend Pattison's explanation [2–8] and the polyester network morphology has been the subject of many papers [9–16].

When the appropriate amount of PVAc is used as a low-profile additive, the mixture is initially miscible. From the beginning of the reaction, UP–styrene copolymer microgels are formed. Microgels are groups of highly crosslinked polyester chains [10]. When these microgels become immiscible, they precipitate. As the microgel concentration increases in the UP-rich phase, the microgels coagulate to form larger particles with a size of about the order of a micron. Fig. 1 depicts the different scales of heterogeneity in the morphology after phase separation in terms of microgels and particles. The macrogelation is the point at which the number of connected particles is high enough to form a continuous phase. The morphology of the polyester network in the presence of PVAc is a two-phase structure more or less bi-continuous consisting of a particle-type polyester phase and the PVAc-rich phase. Near the maximum reaction rate point, microvoids are formed within the thermoplastic phase and there is a general agreement on the role played by these microvoids in the shrinkage compensation [14]. The aim of our paper is to complete the previous descriptions of morphologies involved in the low-profile mechanism.

When the cure of a UP/PVAc/S mixture is performed between two glass slides, the authors noticed by optical microscopy two successive phenomena in that the appearance of a structure of particles precedes a rapid growth of microfissures [2, 4–6]. The morphology of these microfissures has been usually described by the term "dendritic" but fractal geometry is believed to allow a better characterization. Image analysis techniques will be applied to determine the fractal dimension of microfissure binary images. How the microfissures are linked to microvoids has not been discussed by the authors mentioned above. One explanation will be proposed using a computer simulation.

* To whom correspondence should be send.

0022–2461

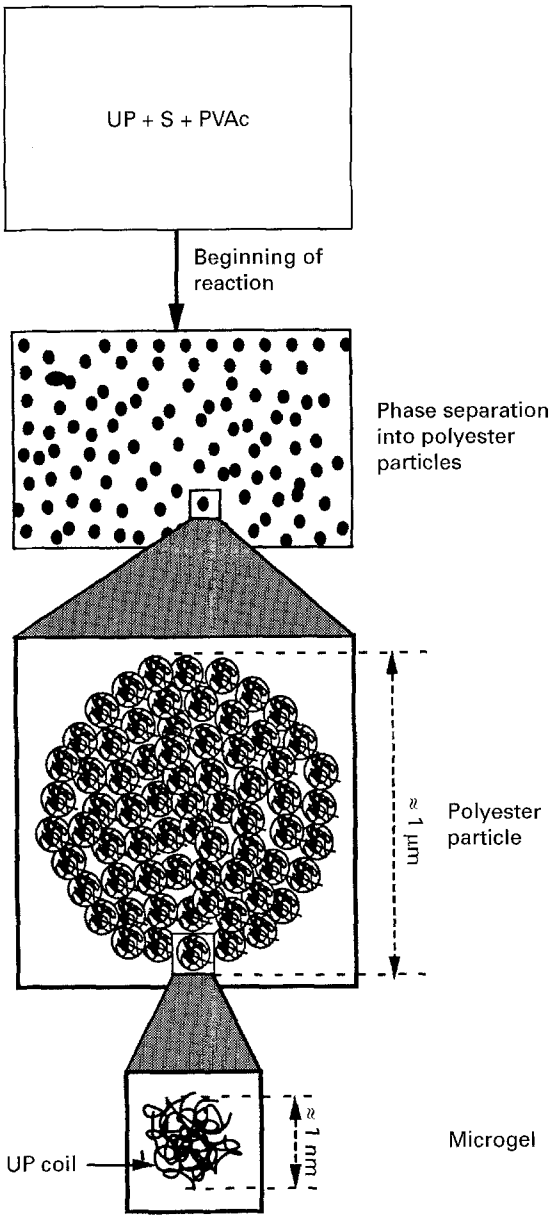

Figure 1 Scheme of the phase separation occurring during cure of a UP/PVAc/S blend.

The general method to characterize the PVAc modified polyester network is to observe the fracture surface after etching by scanning electron microscopy (SEM) [7, 11–15]. The solvent dissolves soluble materials such as PVAc and nonreacted monomers. When viewed by SEM at appropriate magnifications, the polyester network cured with PVAc appears as connected particles. The surface is very rough and can be pictured as a cauliflower. The use of fractal geometry allows us to describe such a morphology. Two methods of computing the fractal dimension of the SEM pictures will be proposed in this paper.

2. Experimental procedure

2.1. Materials

The polyester resin used in this study is a 1:1 copolymer of maleic anhydride and propylene glycol containing 35 wt % styrene (S), MOO4 from Cray Valley (Total). The number average molar mass of the unsaturated polyester prepolymer (UP) is 1500 g mol^{-1} and the equivalent molar mass per mol of double bonds C=C is 156 g mol^{-1} with an average of about 10 vinylene groups per molecule. This UP prepolymer is of a typical SMC grade. The low profile additive investigated is LP40A from Union Carbide which is a 40 wt % styrene solution of PVAc. The unsaturated polyester resin, styrene and low profile additive were used as received without inhibitor removal.

TABLE I Compositions studied

PVA wt %	0	3.2	5	7	10	15
UP wt %	42.4	41.4	40.7	39.9	38.6	36.4
S wt %	57.6	55.4	54.3	53.1	51.4	48.6
N (10^{-3} mol g^{-1})	8.27	8.14	7.83	7.68	7.42	7.0

The compositions studied are listed in Table 1. All the initial blends were miscible at 29 °C and higher temperatures. The different compositions have a styrene molar ratio of 2 with respect to the polyester double bonds (MR), then the total number of reactive double bonds (N) decreases linearly with the PVAc mass fraction.

The t-butyl perbenzoate (TBPB) was used as a high temperature initiator at a concentration of 0.6 g mol^{-1} of double bonds C=C. The addition of 0.17 g mol^{-1} of double bonds C=C of hydroquinone (HQ) was necessary to delay the reaction.

2.2. Optical microscopy and image analysis

The mixture morphology during cure was observed using transmitted light on an optical microscope (Zeiss Axioplan, 12V, 100W, halogen filament lamp). A drop of sample mixture was placed on a microscope slide having carbon fibres as spacer. The cover slip was pressed slightly to spread the resin out into a uniform film with a typical thickness in the range of 10 μm. The sample was then inserted into the microscope hot stage (Mettler FP82) which was used to control the sample temperature. Photomicrographs and image acquisitions were then taken at appropriate times.

2.3. Molded samples and scanning electron microscopy

The mixtures were cured in a molding simulator described elsewhere [17], the plastoreactomat (PRM). The morphology of the reacted samples was studied as a function of the molding conditions and formulations. After PRM molding, the samples were broken and etched in dichloromethane for 30 min. The samples were then gold coated and the fracture surface morphologies were viewed using a SEM (Jeol 840A) at magnifications from 3000 to 10 000x with an accelerating voltage of 10 kV. SEM pictures were then transferred to the computer directly or by using a CCD camera (Pulnix TM 760).

3. Image analysis

A micrograph can be considered as a continuous distribution of grey levels. The transfer of this image information to the computer supposes that it has been digitized: the image is divided into 512×512 pixels with an associated grey level between 0 and 255. Filtering was used in order to eliminate noise. The same ideal low-pass filter was applied to the Fourier transforms of all the images (218×201). The filtered images were then reconstructed by inverse Fourier transform. The magnifications available on an optical microscope do not allow us to discern properly the individual particles and, because of the depth of field, several particle layers are superimposed on the image. However the phase separation can be revealed by using image analysis: band-pass filtering, adaptive thresholding and skeletonation. The diffraction at the fissure surfaces causes the dark appearance but these same areas appear white when viewed with reflected light. The intensity histogram of the filtered image shows a bimodal distribution: the low grey level peak corresponds to the fissures and the high grey level peak to the polyester particles. A binary image is then created using a thresholding technique. The threshold level is chosen at the minimum of the bimodal intensity distribution. The microfissures appear black on the white background.

3.1. Fractal dimension of the microfissures (2-d space)

The microfissures are very similar in shape to the pattern obtained by viscous fingering [18]. The hydrodynamic instability which characterizes the flow of a low viscosity fluid pushing a more viscous fluid into a Hele–Shaw channel leads to highly branched structures. These fingers have been described using fractal geometry. The application of fractals as a mathematical tool for the analysis of rough surfaces or curves has received increasing interest in recent years [19, 20]. Mandelbrot [21] systematized and organized the mathematical ideas concerning such objects. He pointed out that such patterns share a central property which is called self-similarity. These objects are invariant under a transformation which replaces a small part, that is, under a change in scale of the picture. Self-similar structures are called fractals. Fractal objects are usually characterized by their dimension. The measure of a non rectifiable curve is given by a power law such as $L_\lambda \propto \lambda^{1-D}$ where: λ is the gauge length, L_λ is the length of the curve measured using a λ-long gauge, and D is the fractal dimension of the curve.

Many physical objects have fractal structures but not in the strict sense as mathematical objects since they are not self-similar under the whole range of scales and a fractal domain can be defined between the size of the individual constituents and the size of the entire object itself.

In order to characterize the microfissures, the fractal dimension of their contour has been determined. The fractal dimension D is usually computed using image analysis techniques. The basic assumption for the image analysis is that the image of a fractal is fractal itself. Several methods have been summed up in the book of Coster and Chermant [22]. In this work, the image is considered as a subset of the plane. If the subset X is covered, with a minimum covering X_d, by balls of diameter d, the Minkowski dimension can be computed as:

$$\lim_{d \to 0} \left[2 - \frac{\log [\text{area}(X_d)]}{\log d} \right] \tag{1}$$

This expression can be extended to any n-dimensional embedding space:

$$D = \lim_{d \to 0} \left[n - \frac{\log [\text{measure}(X_d)]}{\log d} \right] \tag{2}$$

Some of the techniques of mathematical morphology are used to obtain the contour. The threshold image is eroded with a structuring element (3×3, centred). The contour is the result of the subtraction of these two images. The pixel number of the initial contour is called N_i. The fractal dimension is then determined by means of a program developed especially for this application. The contour is thickened λ times with the same increment and the pixel number N_λ is computed for each increment λ. The plot of $\log(N_\lambda / N_i \cdot \lambda)$ as a function of $\log \lambda$ should give a graph approximated by a straight line with a negative slope which can be interpreted as the quantity $(1 - D_1)$.

3.2. Fractal dimension of the polyester network (3-d space)

Pentland [23] noticed that "the fractal model of imaged 3-d surfaces furnishes an accurate description of most textured and shaded image regions". The feasibility has been demonstrated by Pande *et al.* [24] who showed that the total area of a rough surface using SEM techniques is proportional to the secondary electron yield from this surface. We assume that this principle is true for the surface covered by each pixel. The grey level is regarded as the third spatial dimension.

The fractal dimension of this topological surface is computed using two methods. The first one is based on the same principle as the one employed for the microfissures (see Equation 2 with $n = 3$). The surface is thickened, step by step, by a structuring element ($3 \times 3 \times 3$, centred). The fractal dimension calculated from the slope of the line is called D_1.

The second method studies the relationship between surface area and levels of spatial resolution [25]. Consider 4 pixels A, B, C, D, defining a δ-large square window and let us denote the corresponding grey levels by a, b, c, d and the spatial coordinates of A by i, j. The pixels are then marked out by $A(i, j, a)$ $B(i, j + \delta, b)$ $C(i + \delta, j + \delta, c)$ $D(i + \delta, j, d)$. By a change of origin point, we have $A(0, 0, a)$, $B(0, \delta, b)$, $C(\delta, \delta, c)$, $D(\delta, 0, d)$. The surface area formed by

$ABCD$ is approximated by the sum of both triangular surfaces ABD (S_1) and BCD (S_2).

$$S_1 = \tfrac{1}{2} \| \vec{AB} \wedge \vec{AD} \|$$

$$= \frac{\delta}{2} ((d-a)^2 + (b-a)^2 + \delta^2)^{1/2} \quad (3)$$

$$S_2 = \tfrac{1}{2} \| \vec{CB} \wedge \vec{CD} \|$$

$$= \frac{\delta}{2} ((b-c)^2 + (d-c)^2 + \delta^2)^{1/2} \quad (4)$$

In the particular case of neighbouring pixels, $\delta = 1$ and:

$$S_{i,j} = \tfrac{1}{2} ((d-a)^2 + (b-a)^2 + 1)^{1/2} + ((b-c)^2 + (d-c)^2 + 1)^{1/2} \quad (5)$$

The surface area of the picture is, at the resolution 1:

$$A = \sum_{i=0}^{510} \sum_{j=0}^{510} S_{i,j} \quad (6)$$

The fractal dimension is computed by increasing the pixel size according to a power law ($\lambda = 2$–2^9). The graph $\ln(A_\lambda)$ vs. $\ln(\lambda)$ gives aligned points, the slope of the straight line is denoted β. The fractal dimension obtained with this second method is thus $D_2 = 2 - \beta$.

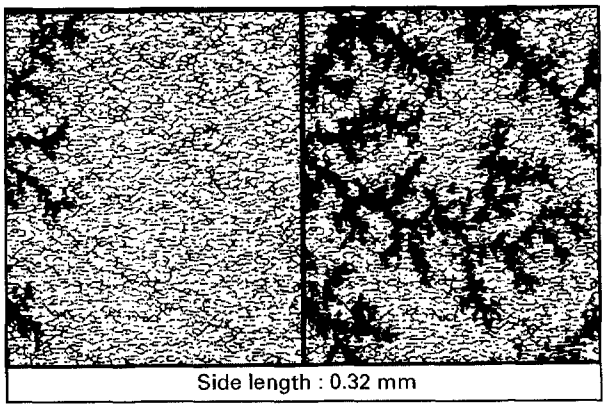

Figure 2 Images of growing microfissures on the phase separated morphology revealed by image processing (15 wt % PVAc, cure temperature = 150 °C).

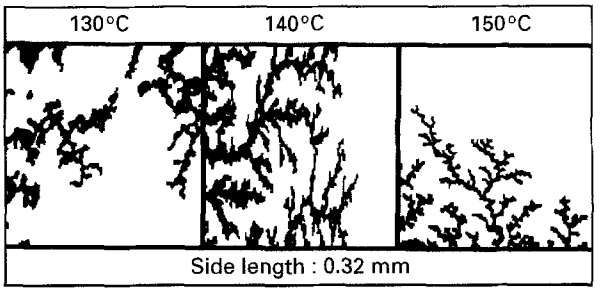

Figure 3 Influence of the curing temperature on microfissuring process for a 15 wt% PVAc blend.

4. Results

4.1. Description of the reaction between two glass slides

When the 15 wt % PVAc mixture is cured between two glass slides, the *phase separation* is observed at the very beginning of the reaction. Afterwards the *fissuring* phenomenon takes place in that a rapid growth of microfissures is observed progressing across the field of the microscope. Several images were acquired showing the growth of the microfissures in the same area. Image analysis techniques were used to highlight the particles resulting from the phase separation and the microfissures. These techniques are described in the experimental section. Fig. 2 shows the superposition of the image of the separated phases and the image of the microfissures at two growth steps.

4.2. Influence of temperature and PVAc content on microfissuring

Because the fissuring is believed to be affected by the curing temperature [4, 5], the 15 wt % PVAc composition was cured at four temperatures: 130, 140, 150 and 165 °C. After phase separation, no fissuring was observed for the reaction at 165 °C. For curing at 130, 140 and 150 °C binary images of the growing microfissures are shown in Fig. 3. As already described by Ross [5], the fissures exhibit more branching and are thinner at high temperatures.

To investigate the effect of the concentration of the low profile additive, mixtures containing 0, 3.2, 5, 7, 10 and 15 wt % PVAc were cured at 150 °C. The reactive system without PVAc exhibited no change during cure. There was no phase separation and the sample remained clear in the microscope field. However some macroscopic and smooth fissures appeared clearly when the sample was viewed with the naked eye. These macrofissures are believed to be the result of polymerization shrinkage. On the other hand, the microfissures are believed to be the cause of shrinkage compensation. For the 3.2 wt % PVAc mixture, no fissuring followed the phase separation. The mixtures with a PVAc content higher than 3.2 wt % were microfissured after the phase separation. The rate of microfissure growth was affected by the reactive system composition. This rate increased as the PVAc content was decreased.

4.3. Fractal characterization of the microfissures

Because of the very rough shape of the microfissures, the fractal concept seems to be appropriate to allow their quantitative description.

The dimension 1 is given to the non microfissuring samples because the smooth line of a macrofissure is a rectifiable curve. Microfissures are actually fractal that is, their dimensions are non integer ($1 < D < 2$). Moreover their dimensions depend on the cure temperature and the PVAc content. Figs 4 and 5 show that the fractal dimension exhibits a trend to augment with increasing cure temperature or PVAc content. This result can be expressed in another way, that the microfissures are more irregular that is, fill more of the

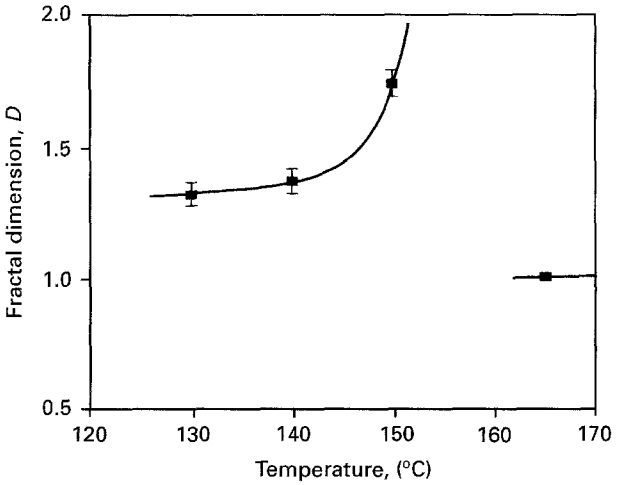

Figure 4 Influence of the curing temperature on the microfissure fractal dimension for a 15 wt % PVAc blend.

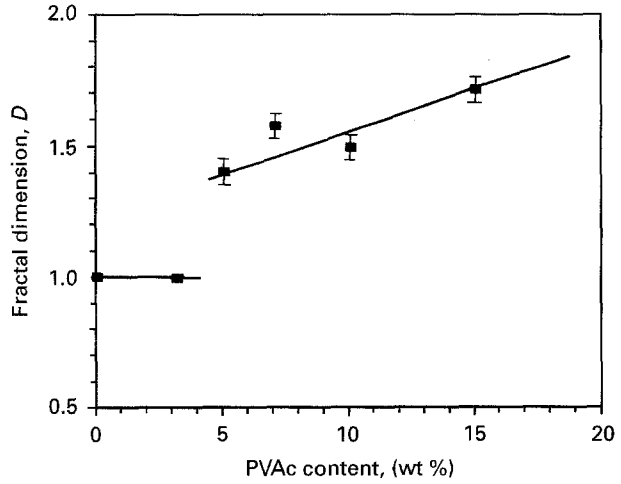

Figure 5 Influence of PVAc content on the microfissure fractal dimension for samples cured at 150 °C.

2-dimensional space as the PVAc content or temperature is increased. It can be assumed that the fractal structure of the microfissures is due to the heterogeneity in the material acting as their support, that is the morphology in separated phases. How this morphology (particle size and fractal dimension) depends on processing conditions is the subject of the following section.

4.4. Description of the polyester network viewed by SEM

Because of its low resolution, the optical microscopy does not allow us to establish a direct link between the subjacent morphology and the microfissures. Therefore, electron microscopy must be used to directly observe the polyester network and the PVAc-rich phase. The microgel size being on the order of one nanometer, the morphology of the network cured without PVAc appears still homogeneous even at a magnification of 10000. However, when PVAc is included in the mixture, the final morphology is completely different in that the polyester network appears as connected particles after PVAc removal. Fig. 6 shows SEM micrographs for the 7 wt % PVAc composition molded with different pressures and temperatures. The morphologies are different with respect to particle size. The UP particles are smaller and more tightly packed as the pressure or temperature is increased. This effect has been observed by other authors [11, 15].

4.5. Fractal characterization of the polyester network

The image of the polyester network is a more or less irregular surface depending on phase separation conditions. With the same approach as used for the microfissures, two image analysis method were applied to assess the fractal dimension of the SEM surfaces. Moreover the roughness of the landscape, R, was computed by $R = \mathrm{Ln}(A/512^2)$.

Table II presents the results concerning the etched surfaces showed in Fig. 6. Particle sizes were measured on the photomicrographs at a magnification of 10000. Table II shows that the roughness increases as the particle size decreases. Moreover the four images are actually fractal because the dimension deduced from the slope is non integer. The first two lines of Table II shows that the size and fractal dimension decrease as pressure is increased whilst the last two lines show that an increase in the temperature increases the fractal dimension determined using the second method (D_2).

Changing the molding parameters modifies the phase separation and hence the resulting polyester network morphology. For instance, increasing the cure temperature leads to a more irregular fracture surface. The SEM surfaces after PVAc removal being fractal, it can be assumed that the polyester-rich phase is itself fractal. Another description is to consider the propagating fissure responsible for break. This fissure propagates in the weakest phase that is the PVAc-rich phase [7], the morphology of which is assumed to be itself fractal and can be described as the negative image of the polyester network. The material morphology can be then depicted as two fractal phases closely fitted into each other. Both experiments, SEM and optical microscopy, allow to qualify the boundary between the polyester phase and the PVAc-rich phase. These assumptions are consistent with the increase in fractal dimension that was observed for the microfissures developed between two glass slides as the cure temperature is increased. According to this description, the fractal dimensions of the microfissures and of the polyester network could be related by a simple law that is demonstrated in the following section.

5. Simulation of the fissuring

With our current knowledge of the system, several attempts were performed in order to simulate the fissuring phenomenon through the polyester network in PVAc/UP/S blends. What was expected from a computer simulation was first, a better understanding of the phenomena by breaking them down into several steps and second, to avoid time consuming

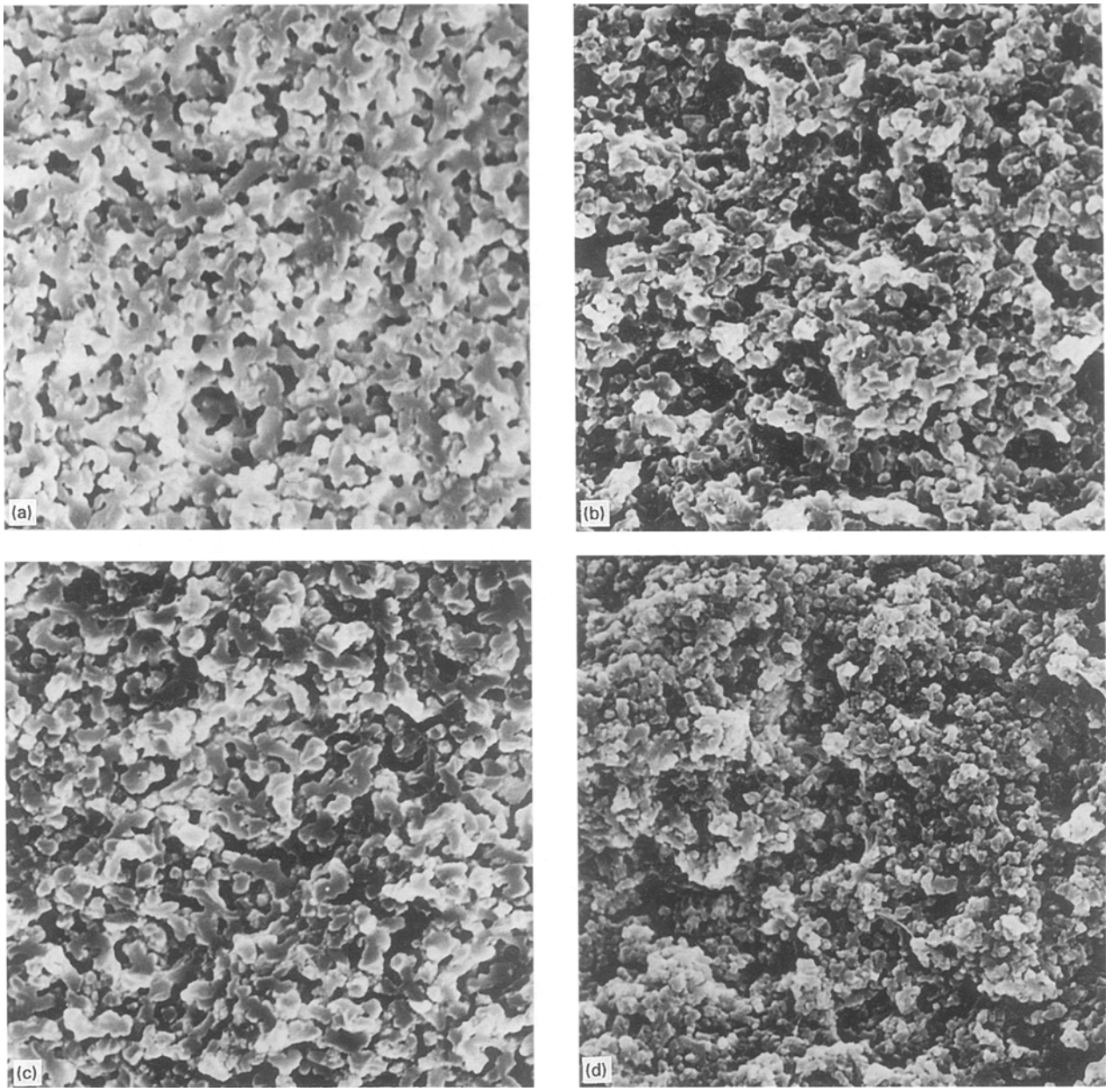

Figure 6 SEM micrographs for the 7 wt % composition molded at: (a) 1.6 MPa, 130 °C, (b) 1.6 MPa, 145 °C, (c) 0.4 MPa, 135 °C, (d) 5.0 MPa, 135 °C (side length 24 μm).

TABLE II SEM surfaces features for the 7 wt % PVAc mixture.

Temperature (°C)	Pressure (MPa)	Fractal dimension		Particle mean size (μm)	Surface roughness R
		D_1	D_2		
135	0.4	2.63	2.80	1.5	1.66
135	5.0	2.57	2.75	0.9	2.60
130	1.6	2.62	2.75	1.4	2.41
145	1.6	2.62	2.80	0.9	2.65

experiments. In the literature, several methods have been described to model fissuring. The first type is deterministic, computed on a square discretization grid with simple mechanical assumptions. Some deterministic models are independent of the material and lead to a unique fractal dimension, 1.65 [26]. Other types take into account the physical/mechanical characteristics of the material [27, 28] but the resulting fractal dimensions are very low (< 1.2) and the fissure patterns are not realistic. The first attempt we made to model the fissures was based on this concept and propagation angles and main directions were measured. Polyester particles were randomly distributed until a given area fraction. A fissure with a potential energy was then initiated and propagated through the particles. When the fissure encountered a particle, the fissure lost a part of its energy and the propagating direction changed. The resulting fissure pattern depended on the particle shape but no realistic fissure was obtained by this deterministic model. Fig. 7 shows an example of pattern obtained by this first model.

The second model, developed in a 2-d space, is based on our interpretation of fractal morphologies described previously. The three main steps of this model are the phase separation into UP particles, microvoid

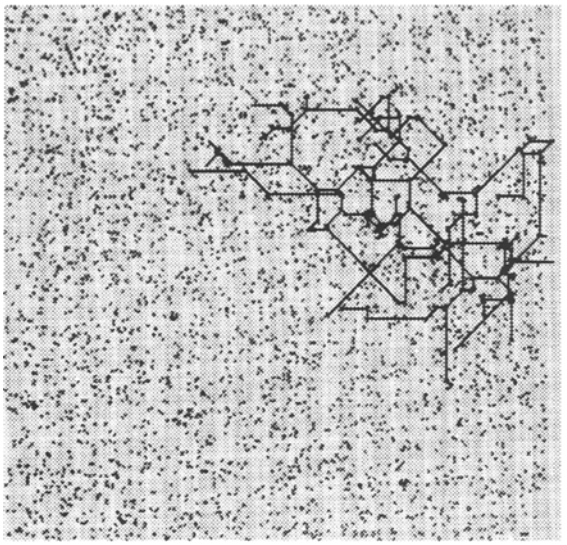

Figure 7 Fissure pattern obtained with the deterministic model.

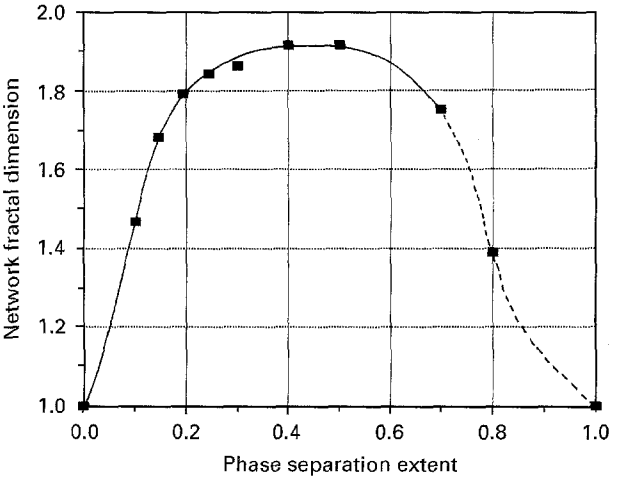

Figure 9 UP network fractal dimension as a function of phase separation extent.

formation followed by propagation into microfissures; all use the diffusion limited aggregation (DLA) model. The DLA is a completely different approach and is believed to be very efficient in the simulation of the growth of fractal objects [29]. This model is based on the addition – step by step and after a Brownian walk – of particles to the growing cluster. DLA clusters are fractal with a measured dimension of 1.76 with the method described above. The construction is irreversible since the particles cannot rearrange after sticking to find a more energetically favourable location. The resulting cluster is characterized by a preferential growth of the ends. One parameter controls the formation rate: the diffusion coefficient of the Brownian motion, D_{iff}, which is usually related to the temperature of the environment.

5.1. Phase separation into UP particles

The phase separation is modelled by growing particle clusters on several germs that are randomly dispersed. 10 germs were used in a 100×100 pixels frame. The parameters controlling the model are:

(1) D_{iff}, particle diffusion coefficient

(2) x_{ps}, phase separation extent, expressed by the surface fraction occupied by particles.

The theoretical maximum value of x_{ps} depends on the additive content. If residual styrene is neglected, it can be assumed, in a rough approach, that $(x_{ps})_{max} = 1 - x_{[PVAc]vol}$, where $x_{[PVAc]vol}$ is the initial volume ratio of the PVAc in the UP/PVAc/S blend.

Fig. 8 shows the different UP networks obtained for various x_{ps}. At the beginning, there are ten objects (particles) that become connected as the cluster grows that is as x_{ps} is increased. The macrogelation occurs when the objects are connected.

The fractal dimension of the UP network was measured with the method described in section 3. As seen in Fig. 9, the fractal dimension of the UP network exhibits a maximum as phase separation occurs until the plateau for $0.3 < x_{ps} < 0.6$. For higher values of x_{ps}, the fractal dimension decreases because the UP network occupies more and more space and the irregular or complex feature disappears.

Surprisingly, D_{iff}, was found to have a negligible effect upon the fractal dimension of the network and its value was then set to 1.

5.2. Microvoid formation in the PVAc-rich phase

Polymerization induces internal stresses that initiate microvoids in the PVAc-rich phase. Microvoids are formed according to a DLA model. The growth of the

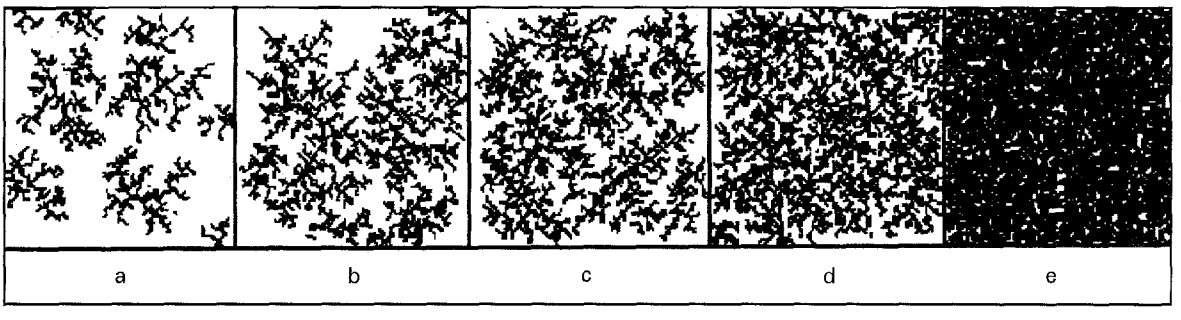

Figure 8 Network morphology as a function of phase separation extent: x_{ps} = (a) 0.15 (b) 0.25 (c) 0.30 (d) 0.40 (e) 0.70.

microvoids stops when it encounters a particle of the UP network that was previously formed. New microvoids are generated until they occupy the chosen fraction area, x_v, where x_v represents the quantity of microvoids that is related to the PVAc-rich phase volume fraction when the microvoids are formed. x_v is directly related to the PVAc efficiency.

5.3. Microvoid propagation into microfissures

The third step is to simulate the 3-d nature of the material in a 2-d frame. The image plan is a material section but the liquid PVAc-rich phase in which the microfissure will propagate is assumed to be connexe in the 3-d space. This description implies that the microvoids will be linked to each other at the end of this propagation step.

One of the microvoids is randomly selected to be at the origin of the microfissure. Then the microfissure propagates according to the DLA model. The change in plan is simulated by restraining the Brownian motion: only the second impact on a particle is efficient to cross over the UP network. In addition any microvoid touched by the microfissure is absorbed. The fissuring phenomenon stops when the chosen fraction area, x_f, is reached. As for x_v, x_f is a parameter related to the PVAc content and increasing the PVAc content is modelled by increasing both x_v and x_f.

Fig. 10 shows the different simulation steps and the very realistic patterns that are obtained by our simulation, compared to the actual microfissures observed by optical microscopy. The fractal dimension of the microfissure was calculated by the same method used for the actual microfissures. As expected, the microfissure geometry depends strongly on the UP network. The correlation between the microfissure and the network fractal dimensions is shown in Fig. 11.

Moreover, the fractal dimension of the microfissures increases with x_f but, as seen in Fig. 12, decreases as x_v is increased. This result is very interesting because it shows a non linear effect of the PVAc content that has already been mentioned in a previous paper [17]. When the UP/S/PVAc blends were cured in the molding simulator, it was noticed that an optimum PVAc content corresponded to the minimum polymerization shrinkage. This optimum in the PVAc content was lowered as the pressure was increased.

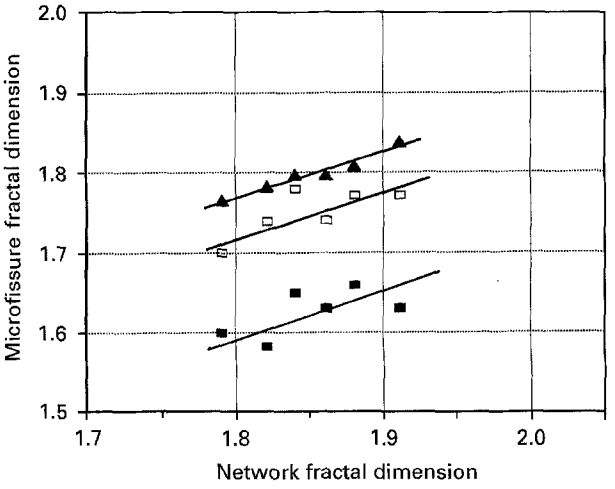

Figure 11 Influence of UP network on the microfissure geometry $x_v = 0.25$ and $x_f =$ (■) 0.15, (□) 0.3, (▲) 0.4.

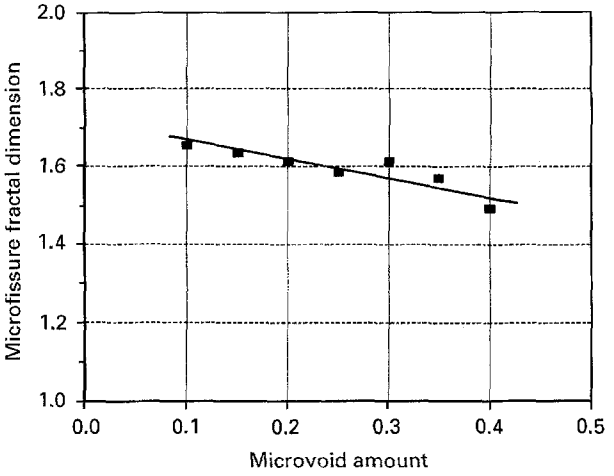

Figure 12 Influence of the microvoid amount on the microfissure geometry $x_{ps} = 0.3$, $x_f = 0.3$.

Microvoids compensate for shrinkage in as far as they are not closed again by the cure pressure and their resistance to pressure is assumed to decrease as the microvoids become larger.

Two conditions are necessary for an efficient low-profile mechanism, (a) the total compensation volume must be high (i.e. big microvoids) but (b) the microvoids must be small to be able to resist pressure. The creation of a fractal volume allows us to achieve these

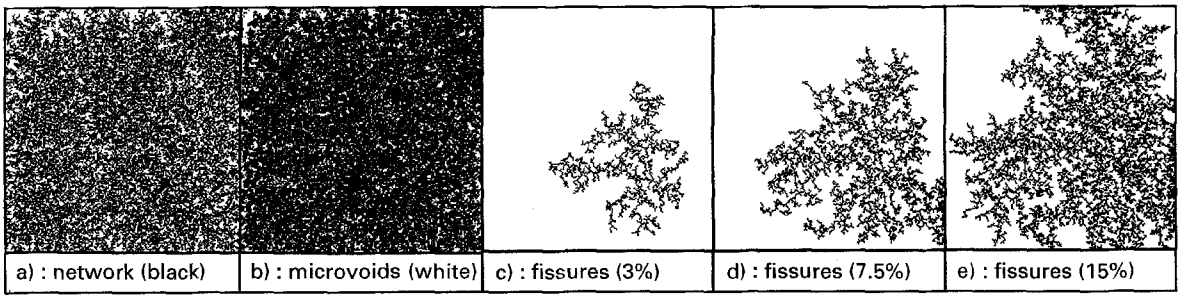

Figure 10 Simulation: (a) of the net work; (b) of the microvoids generated in the separated phase, out of and restricted by the network; (c), (d) and (e): propagation of the microfissures on that medium. (parameters: $x_{ps} = 0.5$, $x_v = 0.25$, $x_f = 0.15$.

contradictory conditions by spreading out the compensation volume amongst different scales. Depending on the phase separation conditions, the size of the PVAc-rich domain can be either more or less favourable for microvoid developement. The fractal dimension of the resulting microfissure is then related to the compensation efficiency: a more divided microfissure, that is a microfissure with a higher dimension, will be more resistant to pressure and thus allows a better compensation.

The model that we have developed to simulate the fissuring well illustrates the necessity to achieve a compromise in the PVAc content. Increasing the PVAc content means an increase in both x_v and x_f and results in two contradictory effects on the microfissure fractal dimension.

6. Conclusions

It is now well recognized that the key to the shrinkage compensation for UP resins used in SMC and BMC is based on the polymer blend morphology resulting from the phase separation. Fractal geometry is a tool for characterizing the peculiar morphologies encountered, and for checking their variations under the physico-chemical conditions of the end-material formation. It is as well known that the shrinkage compensation corresponds with the phenomenon of voids scattered inside the material. In order to show the connection between these voids and the phase separation mechanism, we have performed a simulation.

Although simple, the used method yields very realistic results; so that, one can understand how a compromise has to be found between the following facts:

(a) on one hand optimizing the voids for shrinkage compensation requires a set of voids having a dimension equal to 3,

(b) on the other hand, optimizing their pressure insensivity requires a set dimension equal to 2.

As a result, the shrinkage compensating voids set is fractal, having a non-integer dimension between 2 and 3. This set has grown from the underlying morphology which results from the phase separation, merging the microvoids dispersed in the macro-network anfractuosities.

Acknowledgement

Dr Laurent Suspene, Technical Director, Cook Composites and Polymers Company, Kansas City, is greatly acknowledged for his numerous discussions and helpful advice.

References

1. E. J. BARTKUS and C. H. KROEKEL, *Appl. Poly. Symp.* **15** (1970) 113.
2. V. A. PATTISON, R. R. HINDERSINN and W. T. SCHWARTZ, *J. Appl. Polym. Sci.* **19** (1975) 3045.
3. K. E. ATKINS, "Polymer Blends", D. R. Paul and S. Newman, (Academic Press Inc., London 1978) Vol. 2, pp. 391–413.
4. A. SIEGMAN, M. NARKIS, J. KOST and A. T. DIBENEDETTO, *Intern. J. Polymeric. Mater.* **6** (1978) 217.
5. L. R. ROSS, S. P. HARDEBECK and M. A. BACHMANN, 43rd Annual Conference, Composites Institute, The Society of the Plastics Industry, Inc. Cincinatti, February 1–5, 1988, Session 17-C, 4 p.
6. T. MITANI, H. SHIRAISHI, K. HONDA and G. E. OWEN, 44th Annual Conference, Composites Institute, The Society of the Plastics Industry, Inc. Dallas, February 6–9, 1989, Session 12-F, 11 p.
7. L. SUSPENE, D. FOURQUIER and Y. S. YANG, 45th Annual Conference, Composites Institute, The Society of Plastics Industry, Inc. Washington, February 6–9, 1990, Session 12-F 8 p.
8. C. B. BUCKNALL, I. K. PARTRIDGE and M. J. PHILLIPS, *Polymer* **32** (1991) 636.
9. C. B. BUCKNALL, P. DAVIES and I. K. PARTRIDGE, *ibid.* **26** (1985) 109.
10. Y. S. YANG and L. J. LEE, *ibid.* **29** (1988) 1793.
11. L. KIAEE, Y. S. YANG and L. J. LEE, *AICHE Symp.* **84** (1988) 12.
12. M. KINKELAAR, C. P. HSU and L. J. LEE, 45th Annual Conference, Composites Institute, The Society of the Plastics Industry, Inc. February 12–15, 1990.
13. C. P. HSU, M. KINKELAAR, P. HU and L. J. LEE, *Polym. Eng. Sci.* **31** (1991) 1450.
14. L. SUSPENE, D. FOURQUIER and Y. S. YANG, *Polymer* **32** (1991) 1593.
15. L. SUSPENE and Y. S. YANG, 46th Annual Conference, Composites Institute, The Society of the Plastics Industry, Inc. February 18–21, 1991, Session 7-C, 7 p.
16. C. B. BUCKNALL, I. K. PARTRIDGE and M. J. PHILLIPS, *Polymer* ,**32** (1991) 786.
17. M. RUFFIER, G. MERLE and J. P. PASCAULT, *Polym. Eng. Sci.* **33** (1993) 466.
18. H. VAN DAMME, C. LAROCHE, L. GATINEAU and P. LEVITZ, *J. Phys.* **48** (1987) 1121.
19. J. F. GOUYET, "Physique et structures fractales". (Masson, Paris: 1992) 234.
20. S. BORMAN, Chemical & Engineering News, (1991) April, p. 28–36.
21. B. MANDELBROT, "Les objects fractals" (Flammarion, Pairs 1984) 203.
22. M. COSTER and J. L. CHERMANT, "Precis d'analyse d'images". (Presses du CNRS, Paris 1989) 560.
23. A. PENTLAND, *IEEE Trans. Pattern Anal. Machine Intell.*, **6**(6) (1984) 661.
24. C. S. PANDE, N. LOUAT, R. A. MASUMARA and S. SMITH, *Phil. Mag. Lett.* **55** (1987) 99.
25. R. CREUTZBURG and E. IVANOV "*Lecture Notes in Computer Science*, Vol. 399", (1989) p. 42–51.
26. T. SHIBAYANAGI, O. YAMAMOTO and S. HORI, *Materials Transactions, JIM* **31** (1990) 225.
27. H. TAKAYASU, *Prog. Theor. Phys.* **74** (1985) 1343.
28. H. J. HERRMANN, J. KERTESZ and L. DE ARCANGELIS, *Europhys. Lett.* **10** (1989) 147.
29. L. M. SANDER, *Nature* **322** (1986) 789.

Received 11 July 1994
and accepted 15 December 1995